



UPPSALA
UNIVERSITET

UPTEC W 17 010

Examensarbete 30 hp
Oktober 2017

Experimental and theoretical studies of water droplet surfaces in the presence of glycerol

Experimentella och teoretiska studier av
vattendroppars ytor vid inverkan av glycerol

Anton Nygren

ABSTRACT

Experimental and theoretical studies of water droplet surfaces in the presence of glycerol

Anton Nygren

Water aerosols affect the climate because they have an impact on the radiation balance and cloud formation. Water is present in all forms in the atmosphere (water, ice and steam), for example as rain and hail. Water aerosols play an important role in many biological and chemical processes in the atmosphere. The most common form of water in the atmosphere is water droplets or vapor which often come from oceans and lakes and these aerosols often contain organic compounds. It is therefore interesting to study if organic compounds, in this case glycerol, will be reside on the surface or inside the water droplets. The investigations were performed by using theoretical studies, molecular dynamic simulations in GROMACS, and experimental investigations; X-ray photoelectron spectroscopy with a liquid jet. The experiments were performed at BESSY II, Berlin. The concentrations of glycerol were varied from 75:1; 8:1 to 4:1 (water: glycerol molecules).

The results were that the experiments and simulations indicated that when the concentration of glycerol increased the glycerol concentration at the surface of the water droplet increases until a monolayer of glycerol molecules was formed at the surface. When the monolayer was formed (or close to) less and less glycerol molecules were placed at the water surface and more and more glycerol molecules were placed in the bulk of the water droplet.

Key words: glycerol, water surface, BESSY II, MD, GROMACS, PES, XPS

Degree Project in Environmental and Water Engineering, 1TV962, 30 credits, 2016

Subject reviewer: Olle Björneholm

REFERAT

Experimentella och teoretiska studier av vattendroppars ytor vid inverkan av glycerol

Anton Nygren

Vattenaerosoler påverkar klimatet eftersom de har en inverkan på strålningsbalansen och molnbildningen. Vatten finns i alla former i atmosfären (vatten, is och ånga) som bland annat regn och hagel. Vatten aerosolerna spelar en viktig roll i många kemiska och biologiska processer i atmosfären. Den vanligaste formen av vatten i atmosfären är små vattendroppar eller ånga som ofta kommer från hav och sjöar och som ofta innehåller organiska föreningar. Då vattenaerosoler påverkar klimatet och organiska föreningar är vanligt förekommande i vattendroppar är det intressant att undersöka om organiska föreningar, i detta fall glycerol, hamnar på ytan eller inuti vattnet. Undersökningarna har gjorts genom att använda teoretiska perspektiv, molekylärdynamiska simuleringar i GROMACS, samt experimentella undersökningar i form av röntgen fotoelektron spektroskopi med en vätskejet. Dessa experiment utfördes i BESSY II, Berlin. Koncentrationerna av glycerol varierades från 75:1; 8:1 till 4:1 (vatten: glycerolmolekyler).

Resultaten från experimenten och simuleringarna indikerade att när koncentrationen av glycerol ökade så ökade glycerolkoncentrationen på ytan av vattendroppen tills det bildades ett monolager av glycerolmolekyler på vattenytan. När monolagret hade bildats så placerades mindre och mindre glycerolmolekyler på vattenytan och fler och fler glycerolmolekyler placerades inne i vattendroppen.

Nyckelord: glycerol, vattenytor, BESSY II, MD, GROMACS, PES, XPS

Examensarbete i miljö- och vattenteknik, 1TV962, 30 hp, 2016

Ämnesgranskare: Olle Björneholm

PREFACE

This thesis of 30 credits has been carried out at Uppsala University as a degree project in environmental and water engineering. The supervisors for the project has been Clara Saak (PhD) and Carl Caleman (researcher), subject reviewer was Olle Björneholm (professor), and examiner is Fritjof Fagerlund (senior lecturer).

I would like to thank my supervisors Clara Saak and Carl Caleman and subject reviewer Olle Björneholm as they helped me through this entire project. I also want to thank Isaak Unger (post doc) for helping me throughout the process and Tulio Rucha, Niklas Ottoson, Johannes and the staff at BESSY II for all the help.

POPULÄRVETENSKAPLIG SAMMANFATTNING

I atmosfären finns det små vattendroppar (så kallade vattenaerosoler) som bildas på olika sätt. Ett av dessa är när bubblor på vattenytan av hav och sjöar spricker, efter vilket de små droppar som bildas transporteras upp i atmosfären med hjälp av vind och turbulens.

Vattenaerosolerna kommer i detta fall från vattenkroppar som innehåller organiska ämnen som då kan följa med dropparna och påverka dess fysikaliska (exempelvis ytspänning) och kemiska egenskaper (exempelvis hur vattenaerosolerna reagerar med andra ämnen).

Vattenaerosoler har i sin tur en stark påverkan på strålningsbalansen, det vill säga balansen av ingående strålning från solen och utgående strålningen från jorden eftersom de reflekterar och absorberar strålning samt påverkar molnbildningen. Förändringar av de fysikaliska och kemiska egenskaperna av vattenaerosoler, så som de från hav och sjöar, påverkar hur dessa absorberar eller reflekterar strålningen och kan därför förändra strålningsbalansen och i slutändan vårt klimat. Det är därför viktigt att veta hur vattenaerosolernas egenskaper påverkas av organiska ämnen. Fortsättningsvis påverkar de organiska ämnena i vattenaerosoler egenskaperna hos dropparna på olika sätt beroende på om de hamnar inne i eller på ytan av dropparna och forskning pågår just nu för att ta reda på mer om var olika organiska ämnen hamnar, där denna uppsats är ett bidrag. Eftersom man just nu har bristfällig information om vattenytor och hur de påverkas av organiska ämnen forskas det vidare för att få en bättre förståelse av detta fenomen. Forskningen kan exempelvis göras med något som kallas röntgen fotospektroskopi (XPS), som även är den metod som huvudsakligen beskrivs och används i denna uppsats.

XPS är en teknik som gör det möjligt att studera ytor av olika slag på en molekylär nivå. Metoden går ut på att ljus riktas mot ett provexemplar som i denna uppsats är en vattenstråle i vakuum. Ljuset innehar en vald energi som tillförs till atomerna och gör så att elektroner exciteras, det vill säga hoppar upp till ett skal som utgör en högre energinivå eller helt lämnar provet och rör sig ut från provexemplaret, in i vakuumet. De elektroner som lämnar provexemplaret tar sig sedan in i en analysator. Analysatorn mäter i sin tur rörelseenergin av elektronen och räknar utifrån detta ut bindingsenergin, den energi det krävs för att elektronerna ska lämna sin atom. Bindningsenergin av en elektron är specifik för varje ämne och tillåter därför att man kan utläsa vilka ämnen som ligger på ytan av vattendropparna i strålen som utgör provexemplaret. XPS är en tillförlitlig metod att använda till experiment där ytor undersöks därför att elektroner från atomer som är inne i vattnet stöter ihop med andra atomer och elektroner och därför inte kan röra sig ut ur provexemplaret.

För att kunna jämföra experimenten med teori så utförs ofta teoretiska beräkningar, vilket även är fallet här. De teoretiska beräkningarna som gjordes var simuleringar i programmet Gromacs. Dessa gjordes genom att simulera en "låda" med ett visst antal vatten- och glycerolmolekyler (den organiska molekyl som använts i den här uppsatsen) med vakuum på två sidor av lådan. Positionerna samt densiteten av alla molekyler beräknas i systemet och man kan därefter iaktta var glycerol- och vattenmolekylerna befinner sig i lådan under simuleringen.

I denna uppsats har som sagt glycerol valts som det organiska ämnet att tillföras till vatten och detta eftersom att man vet att glycerol finns och har funnits länge i naturen samt att dess påverkan på vattenaerosoler trots detta har varit svår att bevisa. Resultaten av den här studien visar att experimenten och simuleringarna båda kom fram till att glycerol placerades på ytan av vattendroppar vid låga koncentrationer och att glycerolmolekyler på ytan ökade i antal när glycerolkoncentrationen ökade fram till en viss glycerolkoncentration vid vilken färre glycerolmolekyler åter placerade sig på vattenytan och fler inne i vattenaerosolerna. Anledningen till att färre glycerolmolekyler placerade sig på vattenytan var att vattenytan blev full av glycerolmolekyler och då det blev svårare att få plats på vattenytan började glycerolmolekylerna att placera sig inne i vattendroppen på nytt. Det här

pekar på att glycerol och liknande molekyler kommer att befinna sig på vattenytan av vattendroppen fram tills en viss gräns då det blir för fullt. Detta kommer att leda till en bättre förståelse för hur strålningsbalansen påverkas och i slutändan vårt klimat.

LIST OF ABBREVIATIONS

BE	Binding Energy
HOMO	Highest Occupied Molecular Orbital
HPLC	High Performance Liquid Chromatography
Hν	Energy of photons
KE	Kinetic Energy
MD	Molecular Dynamic
NPT	number of particles, pressure and temperature
NVT	constant Number of particles, Volume and Temperature
PE	Photo Emission
PES	Photo Electron Spectroscopy
POA	Primary Organic Aerosols
SOA	Secondary Organic Aerosols
XPS	X-ray photoelectron spectroscopy

LIST OF FIGURES

- Figure 1.** A description of the three steps of x-ray photoelectron spectroscopy. At step one an electron in a molecule at ground state absorbs a photon and emits the electron. The molecule then goes into a photoionization state. The second step is when the emitted electron moves through the sample to the surface and the third when the emitted electron enters the vacuum surrounding the sample and moves further into analyzer. p. 4
- Figure 2.** A general description of a synchrotron facility with the five main components p. 6
- Figure 3.** Schematics of the apparatus. The important parts are: 1 nozzle source, 2 liquid jet, 3 skimmer, 4 spectrometer entrance, 5 cold trap, 6 sample reservoir (loop system), 7 placement controller of the jet. The x-ray is hitting the water molecules at the red spot p. 7
- Figure 4.** The experimentation station. 1 is the analyzer, 2 is one of the three cold traps, 3 is the chamber with the water jet p. 8
- Figure 5.** A General description of the hemispherical analyzer p. 9
- Figure 6.** The schedule of how the sample reservoir system works. The peristaltic pump is used to pump the sample into the sample reservoir. The high-performance liquid chromatography (HPLC) pumps makes sure the pressure in the sample reservoirs are high enough for the liquid to flow into the jet, refill or waste depending on the settings. When one sample reservoir is connected to the jet the other sample reservoir is connected to either the waste or being refilled p. 10
- Figure 7.** Depicted the 4 steps of making the simulation boxes. 1 is when there was one glycerol molecule in the box, 2 is when the box with one glycerol molecule was multiplied, 3 is when the boxes was filled with the right amount of water and 4 is when the slab was created (one dimension of the box was increased) p. 13
- Figure 8.** The water spectra for the stability measurements of the ratio 1 glycerol: 75 water. The photoelectron intensity is on the y-axis and the binding energy (eV) is on the x-axis p. 14
- Figure 9.** The three spectra of C1s. which are used for the area calculations later. The photoelectron intensity is on the y-axis and the Electron binding energy is in the x-axis (eV) p. 15
- Figure 10.** The plot of the calculated areas of C1s. The red curve is the relative amount of glycerol (the area of glycerol). The green line is the kx-line. The relative amount of glycerol is on the y-axis and the concentration (M) is on the x-axis p. 16
- Figure 11.** The plots of the simulations of the three glycerol: water ratios. 1 is the MD simulation of the 1 glycerol: 75 water ratio, 2 is the MD simulation of the 1 glycerol: 35 water ratio and 3 is the simulation of the 1 glycerol: 8 water simulation. The red lines are the glycerol density and the blue lines are the water densities. The water surfaces are at around 5 nm (where the densities started to decrease towards zero) p. 17
- Figure 12.** The divisions of the highest bulk and surface densities. The division between the highest glycerol density in the bulk and the surface was 0.88 for the 1 glycerol: 75 water, 0.91 for the 1 glycerol: 35 water and 1.01 for the 1 glycerol: 8 water ratio p. 18

LIST OF TABLES

- Table 1.** Ratio of water to glycerol, concentration of glycerol, temperature in tube/at the jet and the weight of water and glycerol used p. 10
- Table 2.** The resolution of Scienta R4000 HiPP-2 analyzer (Scienta, 2016) p. 11
- Table 3.** The three points with the largest difference between them. The points are from the spectrum before and after the measurements of the 1 glycerol:75: water ratio p. 14

TABLE OF CONTENTS

1. INTRODUCTION	1
2. THEORETICAL BACKGROUND.....	2
2.1 ORGANIC MOLECULES IN THE ATMOSPHERE	2
2.2 THE ALCOHOL-WATER INTERFACE	2
2.3 X-RAY PHOTOELECTRON SPECTROSCOPY (XPS)	3
2.3.1 Surface sensitivity	4
2.4 MOLECULAR DYNAMICS (MD).....	4
2.5 SYNCHROTRON RADIATION.....	5
3. METHOD	6
3.1 EXPERIMENTAL SETUP	6
3.1.1 Liquid jet.....	8
3.1.2 Analyser	8
3.2 EXPERIMENTAL MEASUREMENTS.....	9
3.2.1 Calculations of the experimental data.....	11
3.3 MD SIMULATIONS	12
4. RESULTS	14
4.1 STABILITY OF MEASUREMENTS	14
4.2 AREA CALCULATIONS OF C1s SPECTRA	15
4.3 MD SIMULATIONS	16
5. DISCUSSION.....	18
5.1 COMPARISON BETWEEN THE EXPERIMENTS AND SIMULATIONS	18
5.2 LIMITATIONS AND STRENGTH OF STUDY	19
6. CONCLUSION.....	19
7. REFERENCES	20
8. INTERNET REFERENCES	24
APPENDIX A. STABILITY MEASUREMENTS.....	25

1. INTRODUCTION

Aerosols have a relevant influence on the radiation balance (the balance between incoming radiation (mainly from the sun) and outgoing radiation from earth (Rohli and Vega, 2015)) and cloud formation (Prisle et al., 2010) because they have influence on the radiative forcing (describes changes in the radiation balance caused by forcing agents, for example aerosols (Boucher et al., 2013)). The radiative forcing that is calculated is used to predict climate change. The effect of aerosols on the radiative forcing and the interaction with clouds are the largest uncertainties in calculations of the radiative forcing (Boucher et al., 2013). A better understanding of the surface of aerosols at the molecular level may provide more information about the effects of aerosols on the radiative forcing and improve climate models (Prisle et al., 2012). The molecular level of the water surface is important to know because the surface's and the water's chemical composition determines the water aerosols' physical-chemical properties (Walz et al., 2015). Water aerosols are of a special interest because the surface structure of water has an important part in many interface processes (Knipping et al., 2000). For example bonding processes at the surface are affected by the surface structure, amongst others ions on the water surface binds with water but not air (Jungwirth and Tobias, 2006).

Water is present in the atmosphere in all forms (water, ice, vapour) as rain, clouds, hail and plays an important role in many chemical and biological processes in the atmosphere (Goody, 1995). Water is generally not in its pure form but in aqueous solutions as in oceans (Petersen and Saykally, 2006) that cover 70% of the surface of Earth (Goody, 1995). In the atmosphere water is mostly present as small aerosol droplets or vapour. Aerosol droplets can initially come from oceans and lakes due to a spray of small water droplets up into the atmosphere when a water bubble bursts at the surface (Mason, 1954). The water aerosols from bubble bursting are from 5 to 300nm in diameter (Fitzgerald, 1991). Water aerosols can then be transported into the higher layers of the atmosphere by turbulence or wind (Levin and Cotton, 2009). Vapour and small droplets have a high surface-to-volume ratio, that means they are sensitive to changes in the surface (Jungwirth and Tobias, 2006; Prisle et al., 2012). The microscopic properties of water surfaces are not fully known today and researchers are trying to further explain details of the properties of water surfaces (Jungwirth and Tobias, 2006; Petersen and Saykally, 2006).

Water aerosols and cloud droplets consist of 20 to 90 wt% organic compounds (Artaxo et al., 2013; Hallquist et al., 2009) (also contributes to cloud formation). Organic compounds react differently in atmospheric processes depending on whether the organic material is contained at the surface or in the bulk of the water aerosols (Acevedo and Armacost, 2010; Jung and Marcus, 2007). This makes it important to know what the composition of the surface of the water aerosols is like, for the chemical reactions in the atmosphere (Vaida, 2011). One method to examine the molecular level of the water surfaces (electronic structures) is to use X-ray photoelectron spectroscopy (XPS) (Hüfner, 2003). XPS can be used to study the electronic molecular structure and to calculate the binding energy (BE) of electrons (Horio et al., 2012; Seidel et al., 2011). A more detailed understanding of the molecular structure can be achieved by combining experiments and molecular dynamic (MD) simulations (Ottosson, 2011).

The organic molecule investigated in this thesis is glycerol. Glycerol was chosen because it has been known to exist in nature for a long time but the molecular mechanisms it affects has been a challenge to prove (Garcia-Manyes et al., 2009; Yancey et al., 1982). This thesis uses x-ray photoelectron spectroscopy (XPS) with a liquid jet and MD simulations to investigate the placement of glycerol molecules in water droplets.

2. THEORETICAL BACKGROUND

2.1 ORGANIC MOLECULES IN THE ATMOSPHERE

There are two different kinds of organic aerosols, primary organic aerosols (POA) and secondary organic aerosols (SOA). POA are aerosols that are emitted in particulate form, while SOA originates from organic compounds in gas form that oxidize and transform to an aerosol phase (Kanakidou et al., 2005). Further, there are three different ways organic aerosols can be formed, urban sources, biomass burning and biogenic sources (De Gouw and Jimenez, 2009). Urban sources are for example emissions from vehicles, an large POA source (Rogge et al., 1993). However, global models calculates that urban sources of organic aerosols are small compared to biomass burning and biogenic SOA emissions (Kanakidou et al., 2005). The POA emissions from biomass burning depends on the burning conditions and the burning substance (Andreae and Merlet, 2001) while there is a need of more research to determine the SOA emissions from biomass burning, due to differences in laboratory studies and measurements (De Gouw and Jimenez, 2009). Global models showed that biogenic sources of biogenic volatile organic compounds has a significant impact on the SOA emissions (Henze and Seinfeld, 2006; Kanakidou et al., 2005), this also agrees with measurements (Cahill et al., 2006; Claeys et al., 2004). The largest part of the biogenic emissions comes from the tropics where isoprene (emitted from vegetation) and photoproducts of isoprene were large contributors to the organic aerosols (Capes et al., 2009). The aerosols are transported by wind and turbulence (Levin and Cotton, 2009) and with time in the atmosphere they meet and absorb other aerosols (for example water) or condensation will happen (Kleinman et al., 2009). It has also been known for 40 years that organic molecules are present in the surface of oceans (Garrett, 1967; Riley, 1963) and therefor there is a transfer of organic molecules into marine aerosols and the atmosphere (Blanchard, 1964). The composition of marine aerosols is formed in the boundary layer over oceans (Massel, 2007a) where the ocean surface mix with gases (for example oxygen and carbon dioxide) (Massel, 2007b), microorganisms (Orellana and Verdugo, 2003) as well as inorganic and organic chemical compounds (Boehme et al., 1993).

2.2 THE ALCOHOL-WATER INTERFACE

The properties (for example the surface tension) of the interface may be altered when surface active compounds (for example organic compounds) accumulate at the surface. An example of organic compounds that affects the properties of the air-water interface are alcohols. Alcohols decreases the surface tension of alcohol-water solutions (Gliński et al., 1998). Studies of short -chained alcohols (Walz et al., 2016) and alcohol isomers (Walz et al., 2015) showed that when the concentration of alcohol is low the aqueous surface will mainly interact with water molecules and the alkyl chains of the alcohol are parallel to the surface. When the alcohol concentration increases at the surface, more and more alcohol molecules will interact with each and finally a monolayer-like (a closely packed layer of amphiphilic molecules) structure of alcohol molecules will be formed at the water surface. When a monolayer has formed, or close to, the hydroxyl groups will be pointing into the aqueous surface with their hydrogen bonds with water molecules still intact and the hydrophobic alkyl chains sticking out of the water surface (Walz et al., 2016, 2015). Hexane is used in another study that shows that the hydrogen bonding at a hexane-water surface are weaker than at the air-water surface. This indicates that the hydrogen bonds between the organic molecule (hexane) and water are weaker than the hydrogen bond between water molecules (Richmond, 2002). Lastly a study of organic molecules shows that solutes on the water surface wants to form favorable polar interactions with the water molecules and therefore polar sides of the solute molecules will face the water. It is also shown that solutes will lay down on the surface so that Van-der-Waals interactions can be formed between hydrophobic groups and water (Hub et al., 2012).

2.3 X-RAY PHOTOELECTRON SPECTROSCOPY (XPS)

X-ray photoelectron spectroscopy was developed as a tool by Kai Siegbahn at Uppsala university (Siegbahn, 1981). Siegbahn and his co-workers developed this instrument with sufficiently high resolution for specific analysis to be carried out and Siegbahn was awarded the Nobel Prize in Physics in 1981 for the development of the XPS (Van der Heide, 2012). In XPS X-rays are used as the source of exciting photons and in experiments photons can have energies over 1000 eV (Hüfner, 2003). The X-ray energy and line width are chosen to maximise photoemission and to get the optimal spectral resolution. The photons from the X-ray interacts with core electrons and when the energy transfer from the photons is sufficiently high they cause electron emissions (Wagner, 2010). The electron emitted has a kinetic energy (KE) that is the quantity measured in the spectrometer. KE can be calculated by:

$$KE^{\max}=h\nu- \Phi_0 \quad (1)$$

where KE^{\max} is the maximum kinetic energy, $h\nu$ is the energy of the photon and Φ_0 is the work function (a constant depending on the surface of the sample) (Einstein, 1905). The equation can be changed when the energy of the photons is known:

$$h\nu= BE+KE \quad (2)$$

and when KE is measured it is easy to calculate the Binding energy (BE) (Siegbahn et al., 1967).

XPS can be used to study the electronic structure of molecules, solids and surfaces and is used in many different fields such as surface chemistry, material science and solid state physics (Hüfner et al., 2005). BE is element and environment specific (Van der Heide, 2012) and can distinguish valence levels (shallow) and core levels (deep) (Werner, 2015). BE of valence levels are lower, more delocalized than core level, and can participate in chemical bonding and interatomic bonds (Werner, 2015). Valence level electrons can be heavily influenced by the surroundings (for example charge transfer) (Van der Heide, 2012). X-ray sources are used to observe the photoionization of core level electrons (Hüfner, 2003). Because BE is elemental specific, elements can be distinguished in a sample by the BE of core electrons. Core level electrons are localized (Werner, 2015) and the BE of the core levels depends on the chemical state of the sample (Hüfner, 2003) and the direct surroundings of the atom (such as protonation or deprotonation of a COOH group). The difference between the changed BE and the pure elements BE due to the chemical state and the surroundings is called the chemical shift. This chemical shift makes it possible to distinguish between two different chemical environments (for example, CH_3-COOH produce two of the C1s, that is an orbital of carbon, peaks) (Werner, 2015). Because of these properties, the core levels can often be used for chemical analysis that is called electron spectroscopy for chemical analysis or ESCA (Hüfner, 2003). A few assumptions are needed for XPS: sudden approximation, independent particle picture and Born-Oppenheimer approximation. The sudden approximation means that the creation of the photo hole is instant and that there is no interactions between electrons leaving the system and the system itself (Hüfner, 2003)

XPS can be divided in three steps. First, an electron absorbs a photon which excites the electron and the molecule thus emits the electron (if the photon has an energy higher than the BE (Werner, 2015)), illustrated in Figure 1 as the first step. Second, the electron moves through the sample to the surface and third, the electron leaves the sample and moves into a vacuum and into the analyser where it is detected (Hüfner, 2003), depicted in Figure 1 as step two and three. In XPS electrons are released from the core level and can

lead to different states of the ionized species. The state of the ionized species of the particle when an electron leaves the highest occupied molecular orbital (Lalithambika et al., 2016) is stable (the system can't relax further except when it interact with the environment then the system can become highly charged) while an electron from the inner or core valence band will create a valence hole which is unstable. When an electron at the core level leaves the particle, it will create a core hole and a highly unstable atom is formed. However the core hole will be filled in a few femtoseconds. If an electron moves from a higher level (for example from a valence band) to fill the core hole, energy will be released from the molecule. The energy release can occur in two ways, either by releasing a photon (X-ray emission) or by exciting and emitting another electron (Auger decay) (Ottosson, 2011). The auger emission does not depend on the photon energy and is therefore independent of the X-ray source (Wagner, 2010).

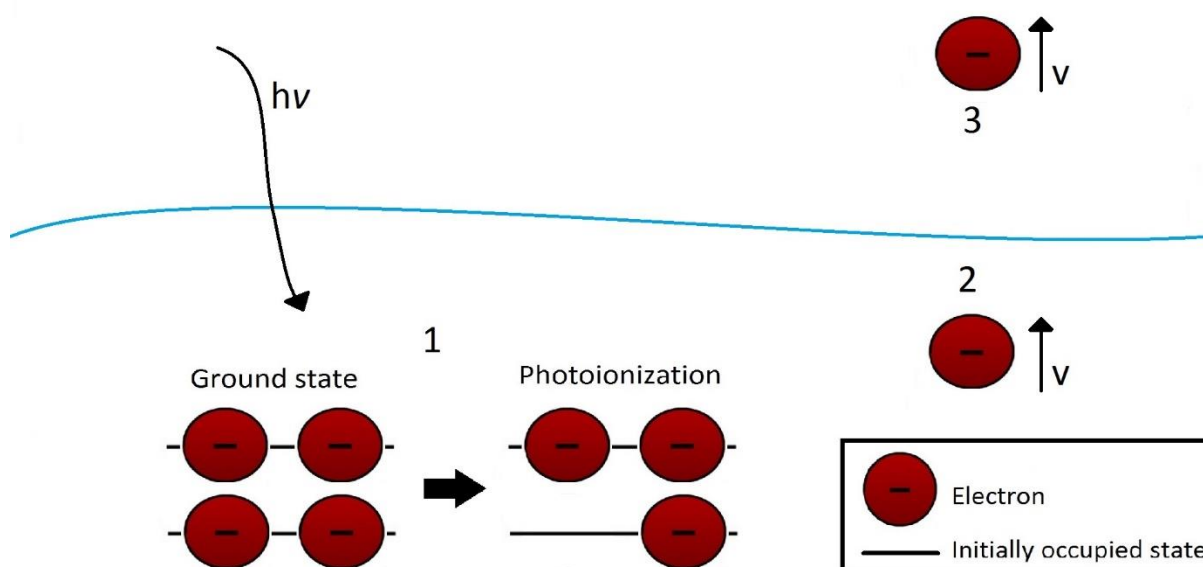


Figure 1. A description of the three steps of x-ray photoelectron spectroscopy. At step one an electron in a molecule at ground state absorbs a photon and emits the electron. The molecule then goes into a photoionization state. The second step is when the emitted electron moves through the sample to the surface and the third when the emitted electron enters the vacuum surrounding the sample and moves further into analyzer.

2.3.1 Surface sensitivity

XPS is commonly used to investigate surfaces of elements. Surface investigations with XPS are used because electrons in the surface of the sample can move without losing energy (Siegbahn et al., 1967). Depending on the energy of the x-ray radiation the radiation can penetrate further down in the bulk of the sample and excite electrons in the bulk (Werner, 2015). However, electrons in the bulk will lose energy due to inelastic collisions with other atoms in the bulk and therefore only electrons from the surface will be released and analyzed in XPS (Siegbahn et al., 1967; Werner, 2015). There are few different ways to measure and calculate the surface sensitivity, for example inelastic mean free path (average distance that an electron can travel before an inelastic collision) (Powell and Jablonski, 2009, 1999).

2.4 MOLECULAR DYNAMICS (MD)

MD is used to describe, get a better understanding of and to predict macroscopic properties of complex chemical systems and is achieved with realistic atom models (Abraham et al., 2015). Atoms are described with a mass, an expansion in the form of a radius and a charge, with bonds as constraints between atoms. The program that was used was Gromacs 5.1.2 (Gromacs and Abraham, 2017). Gromacs was originally developed in the Netherlands at the

university of Groningen but is now being developed in Sweden at Kungliga tekniska högskolan and Uppsala University (Wenger, 2015). MD simulations are calculated with integrations of theoretical physics that are based on Newton's classical equations of motion. Newton's equations are solved using forces from the interaction potentials between molecules in the simulations and the system. The calculations gives the behavior of molecules and atoms over time. The position and speed of the atoms in the system are calculated with defined force fields for every time step of the simulation (Abraham et al., 2015). The force fields are equations that describe the inter and intra molecular interactions (Abraham et al., 2015). In this theses the OPLS/AA force field was selected (Gromacs and Abraham, 2010). Water is calculated with a model of the user's choosing (Wenger, 2015), in this case the SPC/E model (sklogwiki, 2015). The combination of OPLS/AA and SPC/E model was chosen based on the study of Hub et al., (2012) that determined that the combination of OPLS/AA and SPC/E reproduces the right order of Gibbs energy of hydration and therefore they produce a result that can be trusted in this study. SPC/E models the water molecules as a rigid isosceles triangle with charges on all three atoms and the molecule interacts with Coulombic interaction and with Lennard-Jones sites on the oxygen atoms (sklogwiki, 2015). The macroscopic properties and behavior of molecular systems can be distinguished by static equilibrium properties (for example binding constants or the potential energy of the system) and dynamic or non-equilibrium properties (for example the viscosity or the dynamics of phase change). The method to find the macroscopic properties is different depending on if the method is believed to give reliable results and the purpose of the study. The microscopic properties of a molecular system can be found with averages of the properties that is needed (Abraham et al., 2015). For the simulations in this study to work as they should with a canonical ensemble they need to have a constant temperature and therefore a temperature coupling needs to be chosen, there are some built in Gromacs. The relativistic equations can only describe systems with a limited number of atoms at a high quality. Systems with more than a few atoms needs approximations and with larger systems and longer simulations more severe approximations are needed and at one point the approximations needs to be replaced with empirical parameterizations. Also approximations of the interaction potentials (for the solutions of Newton's equations) are needed (Abraham et al., 2015) and the method does generally not describe quantum mechanical phenomena (unless the parameters are given) (Caleman et al., 2012). Therefore the predictions of MD simulations are reliable to a degree but they cannot predict the reality fully, due to the use of classical mechanics and approximations. For example classical mechanics can't describe a system with liquid helium at low temperatures, approximations of the force fields makes so that the force fields can't incorporate polarizabilities and bonded interactions can't be fine-tuned (Abraham et al., 2015).

2.5 SYNCHROTRON RADIATION

Synchrotron radiation is electromagnetic radiation (x-ray radiation) that is emitted by accelerated charged particles and is generated in particle accelerators, a synchrotron (Beaurepaire et al., 2013). The radiation is generated when the electrons are accelerated to velocities close to the speed of light and forced to change their direction (Helms, 2015) in a magnetic field, for example with bending magnets (Beaurepaire et al., 2013).

First, an electron gun with a regular source of electrons, usually generated by thermionic emissions from hot filaments, is needed. The electrons are accelerated with a linear accelerator to approximately 100 MeV. Electrons are then injected into a booster ring (2nd component), Figure 2. The booster ring increases the acceleration of the injected electrons to the energy of the storage ring (3rd component). The electrons are then periodically injected into the storage ring (Figure 2), so that the storage ring contains a

specific current. The storage ring uses magnets to maintain the electrons on a closed path. It has areas with bending magnets that changes the direction of the electrons as well as areas with injector magnets (Willmott, 2011, Figure 2). Injector magnets are sections with alternated succession of magnets, that means that there are more emitters than at the bending magnets (Beaurepaire et al., 2013). The insertion devices generate more intensive synchrotron radiation than bending magnets. When the electrons emit synchrotron radiation the energy of the electrons decreases. The electron energy must be conserved in the system, or the electrons will spiral into the wall and be lost, therefore energy needs to be added. This is done by a radio frequency supply (4th component), Figure 2. The radio frequency supply gives the electrons just the right amount of energy every time they pass through it. The fifth main component is the beamlines. They go tangentially to the bending magnets and along the axes of the insertion devices (Figure 2). The beamlines are then used for different experiments. (Willmott, 2011).

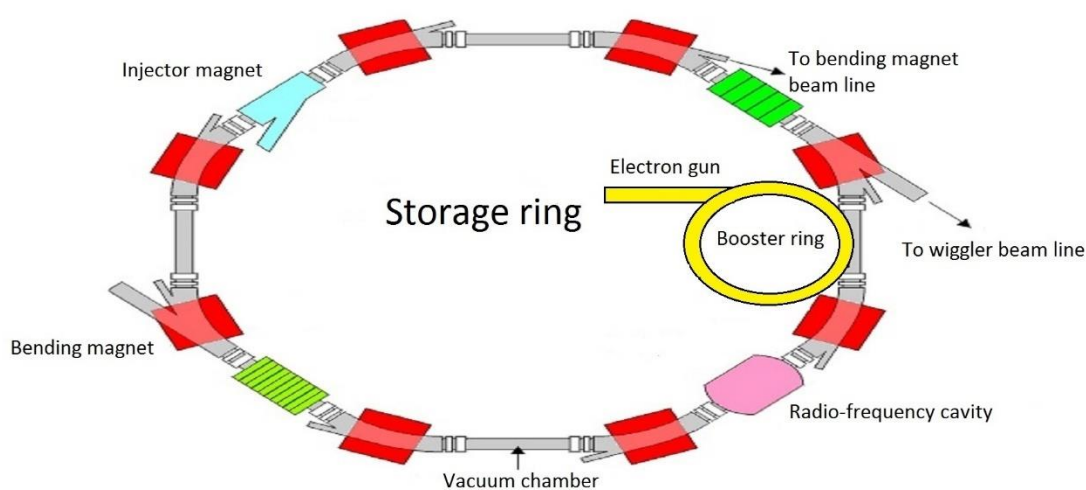


Figure 2. A general description of a synchrotron facility with the five main components

3. METHOD

This chapter describes how the results and information have been collected. There are two different methods that have been used: laboratory experiments and molecular dynamic simulations.

3.1 EXPERIMENTAL SETUP

In experiments with XPS and liquids there is a need of a liquid jet because the sample needs to be renewed regularly so the sample is not contaminated by the surroundings or damaged by the radiation (Werner, 2015). The apparatus for the liquid jet is depicted below in Figure 3 and a photo of the experiment station is depicted in Figure 4. The important parts of the schematics of the apparatus was:

1. nozzle source
2. liquid jet
3. skimmer
4. spectrometer entrance
5. cold trap
6. sample reservoir (loop system)
7. Placement controller of the jet

The x-ray from the synchrotron were hitting the water jet at the red spot in Figure 3. The jet (number 2 in Figure 3) was in a vacuum chamber that usually has a pressure of 10^{-6} to 10^{-8} mbar depending on the diameter of the jet. The pressure needed to be on this level so there was no collisions between electrons and air molecules, so the inelastic mean free path was as large as possible (Faubel et al., 1988). The liquid flowed from a liquid storage (number 6 in Figure 3) to the jet into the nozzle (number 1 in Figure 3) and was shot out through the nozzle into the vacuum chamber. The jet must be started at atmospheric pressure or it will freeze due to cooling when the liquid evaporates. The flow out the nozzle needs to be laminar to get consistent and good readings, however the laminar part is very short and will break up into droplets that freezes (Faubel et al., 1997). After a certain distance the liquid went into a cold trap (Faubel et al., 1988, number 5 in Figure 3) that would “trap” the liquid to make the machine easier to clean.

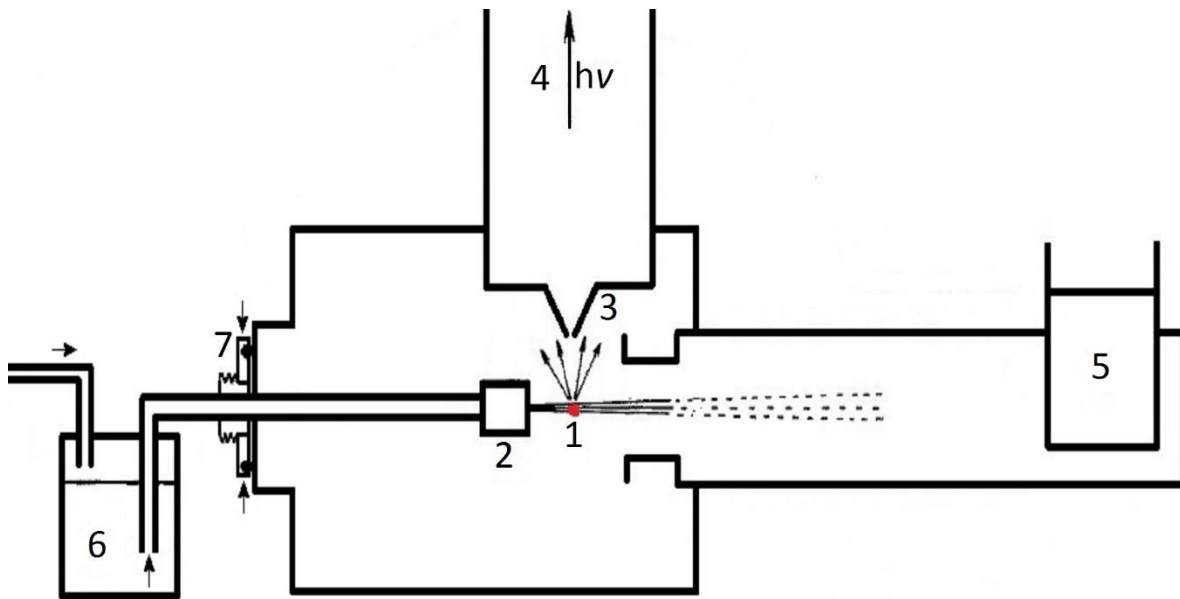


Figure 3. Schematics of the apparatus. The important parts are: 1 nozzle source, 2 liquid jet, 3 skimmer, 4 spectrometer entrance, 5 cold trap, 6 sample reservoir (loop system), 7 placement controller of the jet. The x-ray is hitting the water molecules at the red spot

Figure 4 depicts the experimental station that was used at BESSY II at the beamline U49-2PGM1. (1) is the analyser, while (2) is one of the three cold traps and (3) is the chamber containing the water jet.



Figure 4. The experimentation station. 1 is the analyzer, 2 is one of the three cold traps, 3 is the chamber with the water jet

3.1.1 Liquid jet

A liquid jet is a fast-flowing micro jet and in its set-up it is used in vacuum. The liquid is typically flowing at a velocity of 120 m/s. Its velocity is produced by forcing the liquid at 5-20 bar through a circular glass capillary. The temperature of the liquid is usually 4 °C but can be changed and controlled very precisely. With these settings, the liquid jet will have a smooth beam of liquid which decays into droplets about 5 mm from the nozzle. The diffusion of the liquid has time to achieve equilibrium (between the bulk and the liquid interface) at the laminar region. A stable flow and a smooth surface in the laminar region is needed to be able to measure an undisturbed photoelectron spectrum, which can be achieved with HPLC (high-performance liquid chromatography) pumps. To avoid clogging of the tubes, the solutions are degassed and are often filtered with micro particle filters (Winter, 2009).

3.1.2 Analyser

The electrons emitted in the experiment have a wide range of energies and directions. To collect the emitted electrons, electron optics (a set of electrostatic lenses) are used to focus them into the slit of a hemispherical analyser (Figure 5). To make sure only electrons with a certain kinetic energy can arrive in the middle of the analyser, electric fields are applied. By applying different voltages on the lenses, electrons with different kinetic energies are forced into the slit. The lenses also decelerate or accelerates the initial energy of electrons so the kinetic energy of electrons agrees with the pass energy of the analyser, after passing the entrance slit to the analyser. An energy step size and a dwell time is chosen and the number of electrons reaching the detector is saved as a function of the kinetic energy. The PE spectra is depicted with BE at the x-axis with increasing energies from the right to the left, because the kinetic energies increase with the decreasing binding energies, for example see Figure 8 (Werner, 2015). In this thesis, a spectrum is an energy spectrum. That means the spectrum shows the photoelectron intensity (counts) against the BE in eV. Photoelectron intensity counts are the number of electrons with that specific energy.

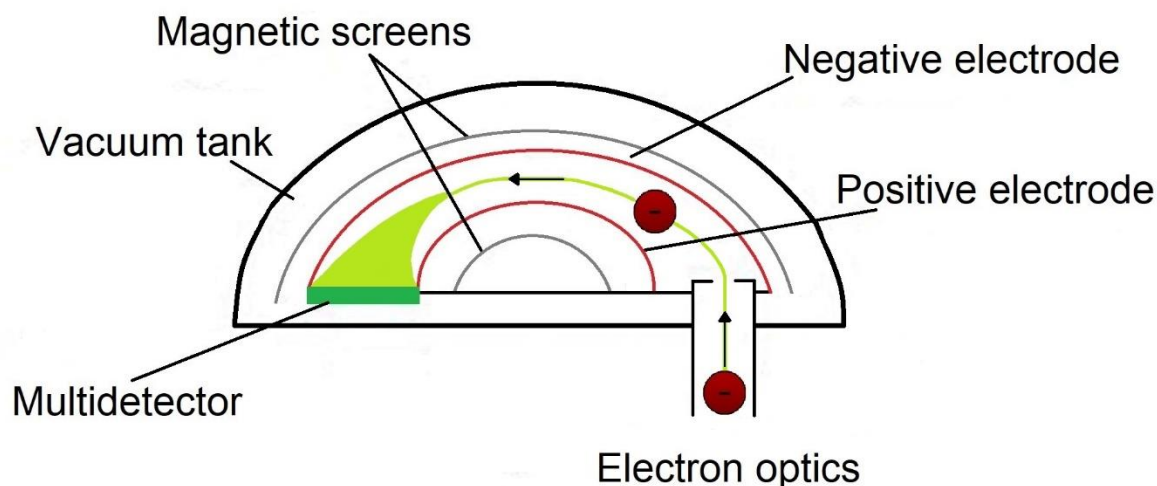


Figure 5. A General description of the hemispherical analyzer

3.2 EXPERIMENTAL MEASUREMENTS

The experiments were performed at BESSY II at Helmholtz zentrum Berlin (HZB) on the 27th of April 2016. The beamline used for the experiment is called U49-2PGM1 (Kachel, 2016). The samples were mixed at the site and an ultra-sonic bath was used to get the sample homogeneous and gas free. Sample reservoirs were used to get the solutions to the jet. The sample reservoir scheme can be seen in Figure 6. The peristaltic pump was used to pump the sample into the sample reservoir. The high-performance liquid chromatography (HPLC) pumps made sure the pressure in the sample reservoirs was high enough for the liquid to flow into the jet/refill/waste, depending on the settings. When one sample reservoir was connected to the jet the other sample reservoir was connected to either the waste or was being refilled. Sample reservoir 1 was always filled with water while sample reservoir 2 had either the sample solution or water in it. The sample reservoirs could contain 75 ml each. The main reason the sample reservoirs were used was to avoid the sample solutions to get into contact with metal parts (for example in pumps). This procedure ensures the longevity of the pumps when using aggressive solutions and to avoid contamination of the sample.

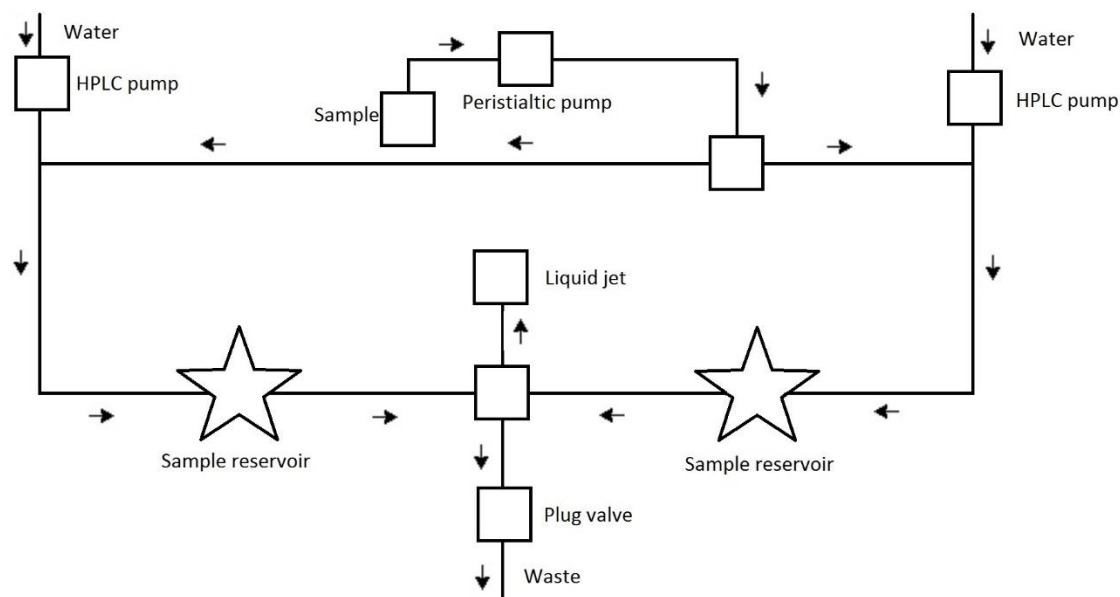


Figure 6. The schedule of how the sample reservoir system works. The peristaltic pump is used to pump the sample into the sample reservoir. The high-performance liquid chromatography (HPLC) pumps makes sure the pressure in the sample reservoirs are high enough for the liquid to flow into the jet, refill or waste depending on the settings. When one sample reservoir is connected to the jet the other sample reservoir is connected to either the waste or being refilled

The temperature of the solutions was measured with a JULABO ED (before the solution reach the jet) and an FLUKE thermocouple thermometer 53/54 II (at the jet). The thermocouple was attached to the jet with copper tape and cable straps. For more information about the thermometers see FLUKE (1999) and Julabo (2013). Before the measurements could start, the pressure in the chamber with the liquid jet needed to be at least in the region of 10^{-4} mbar. The other vacuum areas needed a pressure of at least 10^{-7} mbar. Every time the pressure in the chamber became too high the cold traps needed to be filled and when needed the cold traps and the chamber were cleaned. If ice was formed at the nozzle the chamber was ventilated or if needed the system was cleaned or the nozzle was changed. If the skimmer was dirty or covered with ice (blocked) the system was also cleaned. When the sample was going to enter the jet, a time of 5 minutes elapsed so the water in the jet was replaced by the sample. When a sample was not used sample reservoir 1 was used and water was in the system. The sample in this thesis consisted of glycerol and water. The ratio of water to glycerol molecules is depicted in Table 1, with 75:1 as the lowest water: glycerol ratio and 8:1 as the highest. Table 1 also depicted grams of water and glycerol used, the temperatures, and the concentration in mol.

Table 1. Ratio of water to glycerol, concentration of glycerol, temperature in tube/at the jet and the weight of water and glycerol used

Water (molecules)	Glycerol (molecules)	Water (g)	Glycerol (g)	Concentration (M)	Temperature in tube/at the jet (°C)
75	1	100	6.80	0.74	6/10.0
35	1	100	14.60	1.59	6/10.0
8	1	60	38.36	6.94	6/10.0

The temperature is increased because a higher concentration of glycerol will make the sample more viscous and a higher temperature will make it less viscous and easier to eject from the jet. Before and after every measurement of the samples measurements of

water were done. The measurements of water were done to make stability measurements, to see if something in the experimental set up had change during the measurements of the sample. If something had changed the measurement of the sample had to be remade (Stability of the measurements). The measurement of the sample was done for the C1s orbital, C1s is one of the core orbitals of glycerol. It was chosen because it is only the glycerol that contains this orbital. After the measurements a calculation of the area of the C1s spectra were done (The area calculation procedure).

The program used for the measurement was SES (Hatch, 2005). In this experiment a nozzle with a 22 μm orifice was used with a flowing speed of 0.8 ml/min. The binding energy that was examined was from 284 to 292 eV, pass energy was at 100 eV and the energy was at 600 eV. The analyser slit was at 900 and the spectrometer was a Scienta R4000 HiPP-2, the resolution is specified in Table 2.

Table 2. The resolution of Scienta R4000 HiPP-2 analyzer (Scienta, 2016) and the beamline (Kachel, 2016). The resolution in this thesis was 240 meV at 600 eV

	Resolution at 500 eV/ energy resolution	Resolution at 600 eV/ energy resolution	Resolution at 1500 eV/ energy resolution	Resolution at 5000 eV/ energy resolution	Resolution at 10000 Ev/ energy resolution
Beam line	---/ 25000	240 meV/ 15000	---/ 15000	---	---
Scienta R4000 HiPP-2	15 meV/ ---	---/ ---	---/ ---	40 Ev/ ---	70 Ev/ ---

3.2.1 Calculations of the experimental data

Stability of the measurements

If the measurements were stable the water spectra before and after the measurements were within ~5% from each other. The stability was checked by plotting the water spectra before and after the measurement and a few points were taken to calculate the stability, otherwise it was roughly seen through the plot. This was done in the program Igor pro (WaveMetrics, 2016). If the stability was good the measurements continued but if it was higher than around 5% the measurement that had been done had be taken again.

The area calculation procedure

First a background removal needed to be done. The background is false photoelectron (PE) counts due to electrons that undergo inelastic collisions (for example with other atoms) and therefore loses energy. These background counts deviate from the characteristic energies and should be removed from the data. The background removing was done with Igor pro (WaveMetrics, 2016). Secondly a fitting of the C1s spectra was done so that the area of the fitted curve could be calculated. The fitting was done with another script in Igor pro (WaveMetrics, 2016) and consisted of fitting a curve with the C1s spectra. For the fitting to work as good as possible the data set at the y-axis was needed to be in the 1000 region or lower (or the script was not as efficient), that meant all the data sets needed to be divided by 10000. In the script the number of peaks of the spectra was chosen along with a few other settings. The best fitting was achieved with two peaks (one for the liquid peak and one for the gas peak) for C1s. Since C1s had two peaks it had two fitted curves, one for each peak. The area also (called the relative amount of glycerol of C1s) was calculated by adding the two peaks, because the gas phase peak should not be showing due to negligible evaporation of

glycerol. The area calculations were used to make a plot with the area of the different concentrations. The placement of glycerol could then be determined with the plot of the area change of the C1s and the kx-line, if the C1s plot was not like the kx-line it meant that glycerol was placed at the surface. The kx-line is a linear line with a tilt of one unit per unit and crosses the y axis at zero.

3.3 MD SIMULATIONS

Three MD simulations were performed with GROMACS 5.1.2. The water: glycerol ratio in the simulations were chosen such that it allowed for the studying the effects of an increasing glycerol surface density. The aim was to compare the trends observed in the simulations with those in the experiment. The first simulation had 525 molecules of water and 7 molecules of glycerol (75:1 ratio), the second had 525 molecules of water and 15 molecules of glycerol (35:1 ratio) and the last had 512 molecules of water and 64 molecules of glycerol (8:1 ratio). The force field used in the simulations was OPLS/AA and the water model used was SPC/E. The simulation box of molecules was created in four steps:

1. A box with one glycerol molecule in the middle with vacuum around it was created (step 1 in Figure 7).
2. The box in step one was multiplied and boxes were stacked on top of each other (step 2 in Figure 7).
3. The boxes were filled with water (step 3 in Figure 7).
4. An energy minimization script.
5. An equilibration of the temperature with an ensemble of constant number of particles, volume and temperature (NVT) script.
6. An equilibration of pressure with an ensemble of constant number of particles, pressure and temperature (NPT) script.
7. The dimensions of the box were increased to create a vacuum around the box (step 4 in Figure 7).

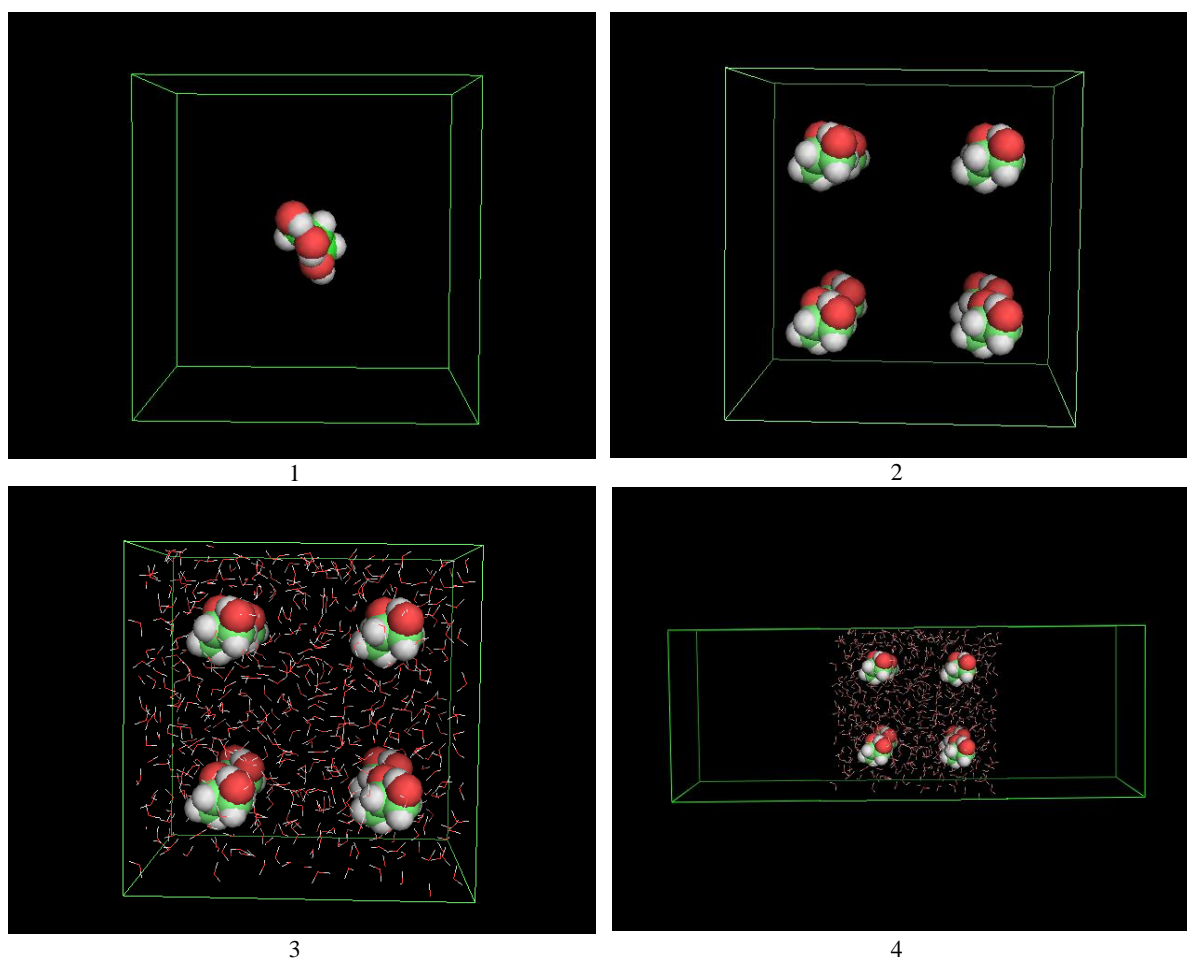


Figure 7. Depicted the 4 steps of making the simulation boxes. 1 is when there was one glycerol molecule in the box, 2 is when the box with one glycerol molecule was multiplied, 3 is when the boxes was filled with the right amount of water and 4 is when the slab was created (one dimension of the box was increased). The Figures were made in PyMOL

The energy minimization was performed to find a starting geometry with the lowest energy. This was achieved by the program moving the position of the atoms to find the local minima of the potential energy. The NVT made sure the simulation structure had the right temperature. The NPT was done to find the dimensions of the boxes. The dimensions of the cubic boxes with molecules was about $2.6 \times 2.6 \times 2.6 \text{ nm}^3$ and the rectangle with vacuum $7.8 \times 2.6 \times 2.6 \text{ nm}^3$. The simulations were done with a 0.002 ps time step and 25000000 steps which makes the total time 50 ns . After the simulations the average density was calculated and normalized. The density plots indicated where molecules were in the box (for example Figure 11). The density is zero when there is vacuum and when the water box density is measured the density increases. This is where the surface of water is and the bulk is where the water density is constant. To easier see the difference between the bulk and surface density of glycerol the highest glycerol density in the bulk and at the surface was divided with each other (Figure 12).

Plots where made in MATLAB R2016a and PyMOL (Schrödinger, 2016) was used to illustrate the boxes and to examine if they behaved as they were supposed to.

4. RESULTS

4.1 STABILITY OF MEASUREMENTS

The measurements below (Figure 8) are an example of the stability measurements for one of the samples (the 1 glycerol: 75 water ratios or the 0.74 M concentration), all the stability measurements can be found in A. The stability measurements were done to know that nothing had changed in the experimental setup during the measurement of the sample. The stability measurements of the 1:75 (glycerol: water) ratio are depicted in Figure 8. The measurements are similar to each other but there is a small difference between them, mostly lower than or around 5% but also a few larger than 5%. For example the three points with the largest difference are given in Table 3. Two of the points had a larger difference than 5%; 7.8% and 6.5%, however the stability is determined with the whole curve and a few points above 5% does not matter

Table 3. The three points with the largest difference between them. The points are from the spectrum before and after the measurements of the 1 glycerol:75: water ratio.

Y coordinate after the measurements	Y coordinate before the measurements	X coordinate	Percentage of the difference between measurements
19787	20692	8.3	4.4
8752.3	9494.4	14.5	7.8
17280	18551	27.7	6.5

The difference is larger at the peaks but decreases directly afterwards. It is always the spectra before the measurements which has the highest values (Figure 8). That means that the set-up has changed slightly and made the resulting in slightly lower measurements than before the sample measurement.

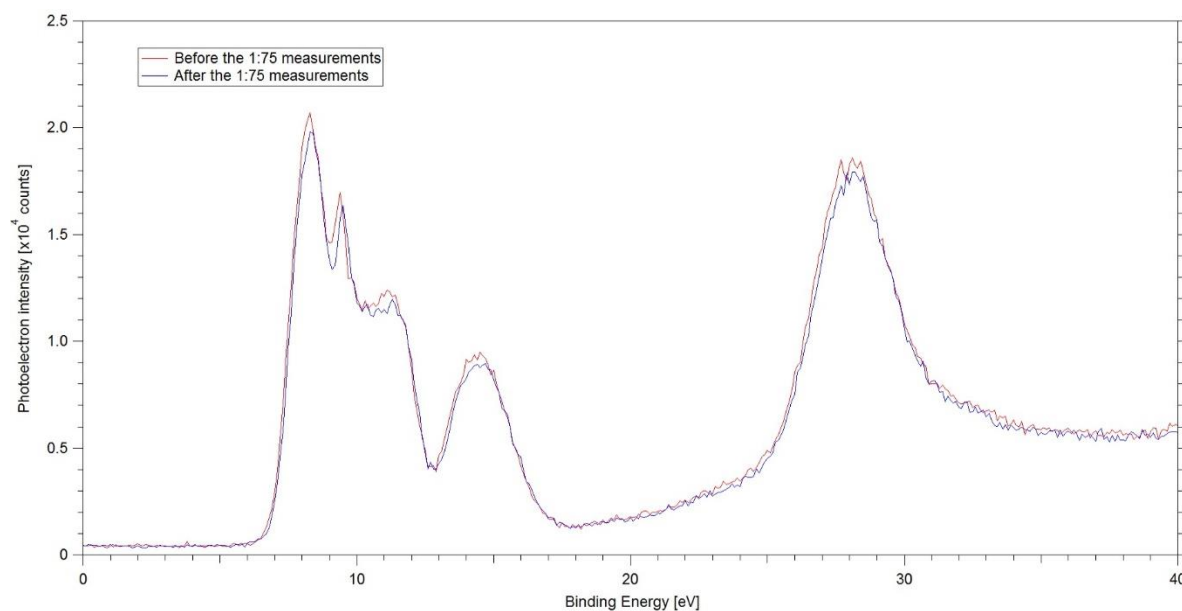


Figure 8. The water spectra for the stability measurements of the ratio 1 glycerol: 75 water. The photoelectron intensity is on the y-axis and the binding energy (eV) is on the x-axis

4.2 AREA CALCULATIONS OF C1s SPECTRA

This section describes the results of the glycerol measurements in the form of a spectra of the C1s orbital (one of the orbitals that only glycerol has and can therefore be a measurement of the glycerol at the surface) with the three different concentrations and the area calculations (see how the area calculations are done in The area calculation procedure) of the spectra. The spectra of the C1s orbital are depicted in Figure 9. The 1 glycerol: 75 water measurements (0.74 M concentration of glycerol) has the lowest photoelectron intensity of all throughout the measurements. The 1 glycerol: 35 water measurements (1.59 M concentration of glycerol) has the largest photoelectron intensity of all the measurements at about 286 eV to 288 eV. At higher BE than 288 eV the 1 glycerol: 8 water measurements (6.94 M concentration of glycerol) had the highest photoelectron intensity (Figure 9).

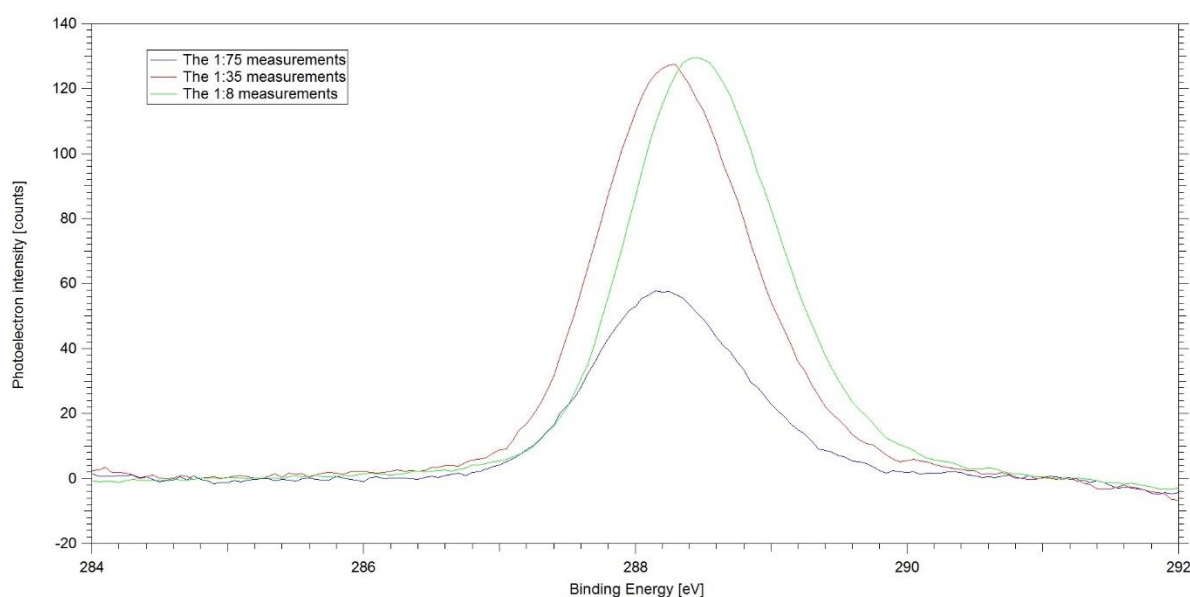


Figure 9. The three spectra of C1s, which are used for the area calculations later. The photoelectron intensity is on the y-axis and the Electron binding energy is in the x-axis (eV)

The 1 glycerol: 75 water measurements (0.74 M concentration of glycerol) had the smallest area (called relative amount of glycerol in Figure 10). The relative amount of glycerol increased with the concentration of glycerol, however the tilt of the curve decreased between the 1.59 and 6.84 M concentration. Therefore the increase in relative amount of glycerol between 1.59 M and 6.94 M is smaller than the increase in relative amount of glycerol from the 0.74 M to 1.59 M concentration. Because of the large tilt of the concentration curve at low concentration and the shift to a smaller tilt at larger concentrations the concentration curve is not similar to the kx-line (Figure 10).

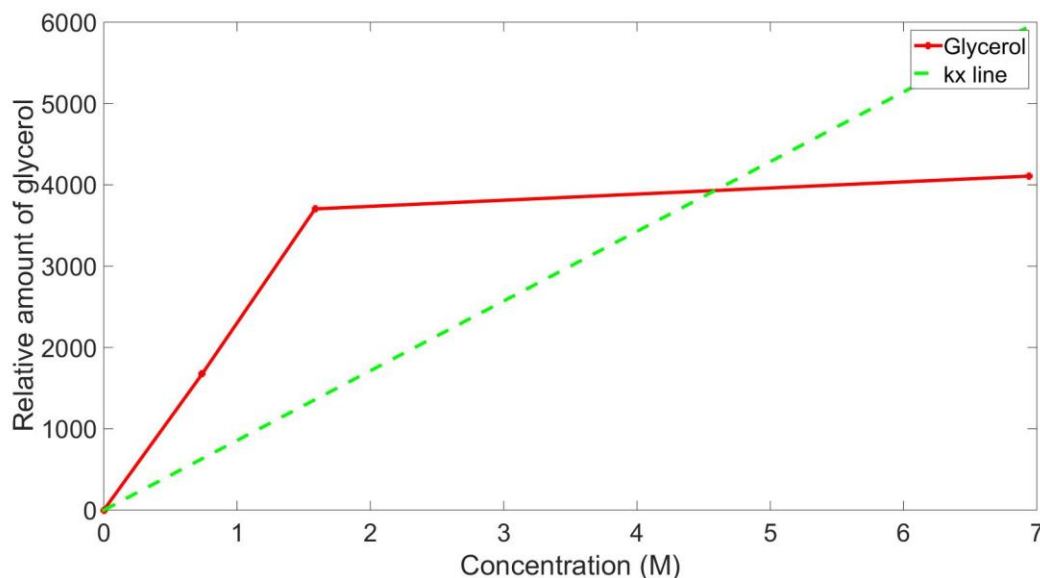
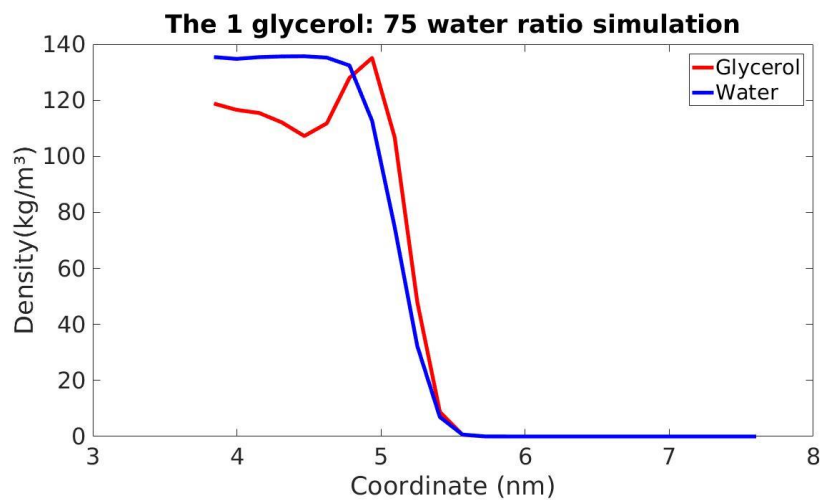


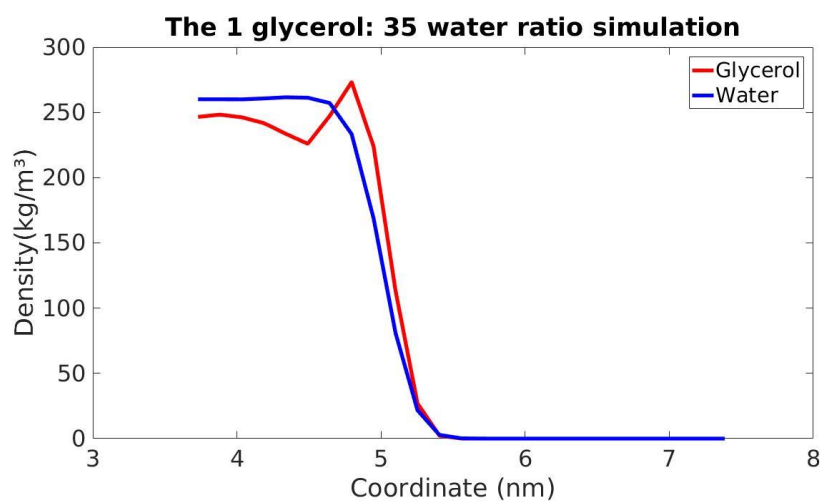
Figure 10. The plot of the calculated areas of CIs. The red curve is the relative amount of glycerol (the area of glycerol). The green line is the kx-line. The relative amount of glycerol is on the y-axis and the concentration (M) is on the x-axis

4.3 MD SIMULATIONS

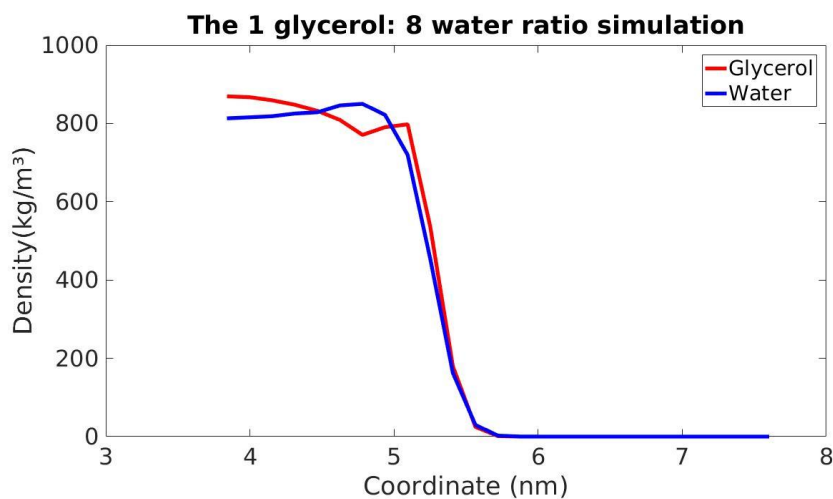
The modelled water densities (the blue lines) and the modelled glycerol densities (the red lines) are depicted in Figure 11. The water density (blue lines) illustrates the borders of the box and the surfaces are at about 5 nm (when the densities starts to go towards zero) and the bulk are from about 4 to 5 nm. Therefore, the only results that will be described here are the glycerol densities (red lines). The 1 glycerol: 75 water ratio simulation depicted that the glycerol density at the surface were larger than in the bulk of the water box. Inside the box between about 4 nm and 4.5 nm the glycerol density decreases but after about 4.5 nm the glycerol density starts to increase and peaks at the surface of the box (1 in Figure 11). The curve of the 1 glycerol: 35 water ratio simulation has about the same shape at the surface (at about 5 nm) as the 1 glycerol :75 water simulation. In the bulk the glycerol density has increased but there is still a peak in the bulk around 4 nm with a decrease until about 4.5 m, where the glycerol density increased and peak at the surface (2 in Figure 11). The density profile for the 1 glycerol: 8 water ratio (3 in Figure 11) had a larger peak in the bulk than the other simulations and as in the other simulations the glycerol density decreases, but in this simulation the minima of the glycerol in the bulk was reached closer to 4.8 nm and then started to increase again and peak at the surface. The difference between the two other simulations is that in the 1 glycerol: 8 water simulation the bulk density was larger than the peak at the surface (3 in Figure 11) and close to the surface there is a small peak in the water density, at around 5 nm.



1



2



3

Figure 11. The plots of the simulations of the three glycerol: water ratios. 1 is the MD simulation of the 1 glycerol: 75 water ratio, 2 is the MD simulation of the 1 glycerol: 35 water ratio and 3 is the simulation of the 1 glycerol: 8 water simulation. The red lines are the glycerol density and the blue lines are the water densities. The water surfaces are at around 5 nm (where the densities started to decrease towards zero). The plots show the average of the two sides of the box

The density in the bulk increased for every measurement with the largest increases between the 1 glycerol: 75 water and 1 glycerol: 35 water simulations and then had a smaller increase between the 1 glycerol: 35 water and 1 glycerol: 8 water simulations (Figure 12).

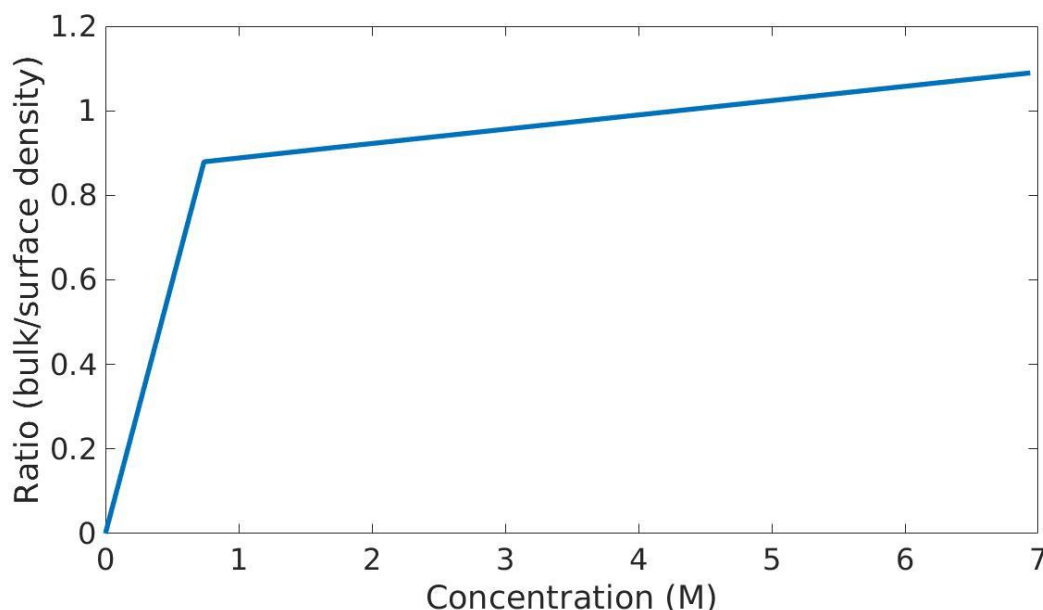


Figure 12. The divisions of the highest bulk and surface densities. The division between the highest glycerol density in the bulk and the surface was 0.88 for the 1 glycerol: 75 water, 0.91 for the 1 glycerol: 35 water and 1.01 for the 1 glycerol: 8 water ratio

5. DISCUSSION

5.1 COMPARISON BETWEEN THE EXPERIMENTS AND SIMULATIONS

The experiments and simulations both agreed that the glycerol molecules below the ratio of 1 glycerol: 35 water (or the 1.59 M concentration) were mostly placed at the surface of the water. This can be seen in the results of the experiments (in Figure 10 where the relative amount of glycerol had a large increase from zero until 1.59 M concentration) and in the results of the simulations of the 1 glycerol: 75 water and 1 glycerol: 35 water (1 and 2 in Figure 11 that depicted that glycerol is mainly at the surface of the simulation box with peaks at the surfaces). The experiments and simulations also agreed that with increasing concentration of glycerol in water the glycerol molecules at the surface increased, however at higher ratios than 1 glycerol: 35 water (or the concentration of 1.59 M) it seems like less and less glycerol molecules are placed at the water surface (Figure 10, Figure 11). Figure 10 (the experiment) depicted that the tilt of the relative amount of glycerol decreased and less glycerol molecules were placed at the water surface and more are placed in the bulk. This agreed with the simulations that showed that the 1 glycerol: 8 water ratio (the 6.94 M concentration) had the same or a bit lower glycerol density at the surface of the water than the glycerol density in the bulk water (3 in Figure 11), this was not depicted in lower water: glycerol ratios (1 and to in Figure 11). This means that both the experiments and the simulations indicates that the theory in 2.2 T has occurred in this thesis. This may also indicate that the same event as in the studies of short-chained alcohols (Walz et al., 2016) and alcohol isomers (Walz et al., 2015) also occurred in this thesis (that the hydroxyl groups are pointing into the water surface).

The simulations also showed that with the increasing glycerol: water ratio the density in the bulk increased (Figure 12). The density profile of the 1 glycerol: 75: water (1 in Figure 11) and 1 glycerol: 35 water (2 in Figure 11) had about the same shape at the surface but in the bulk the glycerol density was higher in the 1 glycerol: 35 water simulation. In the 1

glycerol 8 water density profile (3 in Figure 11) the glycerol density in the bulk had increased even more than the other simulations (Figure 12). This may have indicated that the monolayer had started to form somewhere between the 0.74 M (1 glycerol: 75 water) and 1.59 M (1 glycerol: 35 water) concentration. Except the peaks of the density of glycerol in the 1 glycerol: 8 water simulation there was also a peak in the water density. The water density peak was at the same coordinates (about 4.8 nm) as the minima of the glycerol density. That may mean that the glycerol molecules were gathered together in the bulk and pushed out the water from the bulk closer to the surface.

5.2 LIMITATIONS AND STRENGTH OF STUDY

The strength of the study is that the experiments has been done with high resolution technology and the simulations has been made with a program that is being developed for this kind of calculations. This means that the experiment and the simulations can be compared to see if they agreed with each other. They can then be compared with the theory and a result with good credibility can be achieved.

The simulations where calculated with a cubic box with the length of 2.6 nm while the water aerosols in the atmosphere are at least 5 nm (see I), this means that the simulation boxes should be almost twice as big to better represent reality. The simulations were also made with boxes while in reality water droplets are close to spherical. To be able to do simulations of larger dimensions there is a need of a more powerful computer or a cluster. Water aerosols do not only contain water and glycerol but many other molecules. Most of the water molecules are originally from oceans, this means that the water aerosols have a high probability of containing salts and other molecules from the ocean. The other molecules that the water may contain may affect the glycerol in other ways than only water molecules do. For a more realistic environment there may be a need of experiments with laboratory generated water aerosols with bubble-bursting methods on water containing salts and other molecules that are present in oceans and simulations with the same molecules.

6. CONCLUSION

The experiment and simulations indicated that glycerol molecules were placed at the surface of the water at low concentrations of glycerol. They also indicated that when the concentration of glycerol increased the glycerol concentration at the surface of the water droplet increases until a monolayer was formed, or close too. When the monolayer was formed less and less glycerol molecules were placed at the water surface and more and more glycerol molecules were placed in the bulk of the water droplet. This will help to understand how the radiation balance is affected due to organic molecules in water aerosols and in the end our climate.

7. REFERENCES

- Abraham, M.J., van der Spoel, D., Lindahl, E., Hess, B., *GROMACS development team*, 2015. *GROMACS User Manual version 5.0.7*.
- Acevedo, O., Armacost, K., 2010. Claisen Rearrangements: Insight into Solvent Effects and “on Water” Reactivity from QM/MM Simulations. *J. Am. Chem. Soc.* 132, 1966–1975. doi:10.1021/ja908680c
- Andreae, M.O., Merlet, P., 2001. Emission of trace gases and aerosols from biomass burning. *Glob. Biogeochem. Cycles* 15, 955–966. doi:10.1029/2000GB001382
- Artaxo, P., V. Rizzo, L., F. Brito, J., J. Barbosa, H.M., Arana, A., T. Sena, E., G. Cirino, G., Bastos, W., T. Martin, S., O. Andreae, M., 2013. Atmospheric aerosols in Amazonia and land use change: from natural biogenic to biomass burning conditions. *Faraday Discuss.* 165, 203–235. doi:10.1039/C3FD00052D
- Beaurepaire, E., Bulou, H., Joly, L., 2013. *Magnetism and Synchrotron Radiation: Towards the Fourth Generation Light Sources*, Springer Proceedings in Physics. Springer.
- Blanchard, D.C., 1964. Sea-to-Air Transport of Surface Active Material. *Science* 146, 396–397.
- Boehme, J., Frischer, M.E., Jiang, S.C., Kellogg, C.A., 1993. Viruses, bacterioplankton, and phytoplankton in the southeastern Gulf of Mexico: distribution and contribution to oceanic DNA pools. *Mar. Ecol. Prog. Ser.* 97, 1–10.
- Boucher, O., D. Randall, P. Artaxo, C. Bretherton, G. Feingold, P. Forster, V.-M. Kerminen, Y. Kondo, H. Liao, U. Lohmann, P. Rasch, S.K. Satheesh, S. Sherwood, B. Stevens and X.Y. Zhang, 2013: *Clouds and Aerosols*. In: *Climate Change 2013: The Physical Science Basis*. Contribution of Working Group I to the Fifth Assessment Report of the Intergovernmental Panel on Climate Change [Stocker, T.F., D. Qin, G.-K. Plattner, M. Tignor, S.K. Allen, J. Boschung, A. Nauels, Y. Xia, V. Bex and P.M. Midgley (eds.)]. Cambridge University Press, Cambridge, United Kingdom and New York, NY, USA.
- Cahill, T.M., Seaman, V.Y., Charles, M.J., Holzinger, R., Goldstein, A.H., 2006. Secondary organic aerosols formed from oxidation of biogenic volatile organic compounds in the Sierra Nevada Mountains of California. *J. Geophys. Res.* 111. doi:10.1029/2006JD007178
- Caleman, C., van Maaren, P.J., Hong, M., Hub, J.S., Costa, L.T., van der Spoel, D., 2012. Force Field Benchmark of Organic Liquids: Density, Enthalpy of Vaporization, Heat Capacities, Surface Tension, Isothermal Compressibility, Volumetric Expansion Coefficient, and Dielectric Constant. *J. Chem. Theory Comput.* 8, 61–74. doi:10.1021/ct200731v
- Capes, G., Murphy, J.G., Reeves, C.E., McQuaid, J.B., Hamilton, J.F., Hopkins, J.R., Crosier, J., Williams, P.I., Coe, H., 2009. Secondary organic aerosol from biogenic VOCs over West Africa during AMMA. *Atmos Chem Phys* 9, 3841–3850. doi:10.5194/acp-9-3841-2009
- Claeys, M., Graham, B., Vas, G., Wang, W., 2004. Formation of Secondary Organic Aerosols Through Photooxidation of Isoprene. *Science* 303, 1173. doi:10.1126/science.1092805
- De Gouw, J., Jimenez, J.L., 2009. Organic Aerosols in the Earth’s Atmosphere. *Environ. Sci. Technol.* 43, 7614–7618. doi:10.1021/es9006004
- Einstein, A., 1905. Concerning an Heuristic Point of View Toward the Emission and Transformation of Light. *Ann. Phys.* 17, 132–148.
- Faubel, M., Schlemmer, S., Toennies, J.P., 1988. A molecular beam study of the evaporation of water from a liquid jet. *Z. Für Phys. At. Mol. Clust.* 10, 269–277. doi:10.1007/BF01384861

- Faubel, M., Steiner, B., Toennies, J.P., 1997. Photoelectron spectroscopy of liquid water, some alcohols, and pure nonane in free micro jets. *J. Chem. Phys.* 106, 9013–9031. doi:10.1063/1.474034
- Fitzgerald, J.W., 1991. Marine aerosols: A review. *Atmospheric Environ. Part Gen. Top.* 25, 533–545. doi:10.1016/0960-1686(91)90050-H
- FLUKE, 1999. *51, 52, 53, 54 Series II: Thermometer, Service Manual.*
- Garcia-Manyes, S., Dougan, L., Fernández, J.M., Fersht, A., 2009. Osmolyte-Induced Separation of the Mechanical Folding Phases of Ubiquitin. *Proc. Natl. Acad. Sci. U. S. A.* 106, 10540–10545.
- Garrett, W.D., 1967. The organic chemical composition of the ocean surface. *Deep Sea Res. Oceanogr. Abstr.* 14, 221–227. doi:10.1016/0011-7471(67)90007-1
- Gliński, J., Chavepeyer, G., Platten, J.-K., Smet, P., 1998. Surface properties of diluted aqueous solutions of normal short-chained alcohols. *J. Chem. Phys.* 109, 5050–5053. doi:10.1063/1.477118
- Goody, R., 1995. *Principles of Atmospheric Physics and Chemistry.* Oxford University Press, Oxford, New York.
- Hallquist, M., Wenger, J.C., Baltensperger, U., Rudich, Y., Simpson, D., Claeys, M., Dommen, J., Donahue, N.M., George, C., Goldstein, A.H., Hamilton, J.F., Herrmann, H., Hoffmann, T., Iinuma, Y., Jang, M., Jenkin, M.E., Jimenez, J.L., Kiendler-Scharr, A., Maenhaut, W., McFiggans, G., Mentel, T.F., Monod, A., Prévôt, A.S.H., Seinfeld, J.H., Surratt, J.D., Szmigielski, R., Wildt, J., 2009. The formation, properties and impact of secondary organic aerosol: current and emerging issues. *Atmos Chem Phys* 9, 5155–5236. doi:10.5194/acp-9-5155-2009
- Hatch, R., 2005. *Documentation for Motion and Beamline Control for Scienta.*
- Henze, D.K., Seinfeld, J.H., 2006. Global secondary organic aerosol from isoprene oxidation. *Geophys. Res. Lett.* 33. doi:10.1029/2006GL025976
- Horio, T., Shen, H., Adachi, S., Suzuki, T., 2012. Photoelectron spectra of solvated electrons in bulk water, methanol, and ethanol. *Chem. Phys. Lett.* 535, 12–16. doi:10.1016/j.cplett.2012.03.051
- Hub, J.S., Caleman, C., van der Spoel, D., 2012. Organic molecules on the surface of water droplets--an energetic perspective. *Phys. Chem. Chem. Phys. PCCP* 14, 9537–9545. doi:10.1039/c2cp40483d
- Hüfner, S., 2003. *Photoelectron Spectroscopy, Advanced Texts in Physics.* Springer, Berlin, Heidelberg.
- Hüfner, S., Schmidt, S., Reinert, F., 2005. Photoelectron spectroscopy—An overview. *Nucl. Instrum. Methods Phys. Res. Sect. Accel. Spectrometers Detect. Assoc. Equip., Proceedings of the Workshop on Hard X-ray Photoelectron Spectroscopy HAX PES Proceedings of the Workshop on Hard X-ray Photoelectron Spectroscopy* 547, 8–23. doi:10.1016/j.nima.2005.05.008
- Julabo, 2013. *Operating manual Heating Immersion Circulator ED.*
- Jung, Y., Marcus, R.A., 2007. On the Theory of Organic Catalysis “on Water.” *J. Am. Chem. Soc.* 129, 5492–5502. doi:10.1021/ja068120f
- Jungwirth, P., Tobias, D.J., 2006. Specific Ion Effects at the Air/Water Interface. *Chem. Rev.* 106, 1259–1281. doi:10.1021/cr0403741
- Kachel, T., 2016. The plane grating monochromator beamline U49-2 PGM-1 at BESSY II. *J. Large-Scale Res. Facil. JLSRF* 2. doi:10.17815/jlsrf-2-75
- Kanakidou, M., Seinfeld, J.H., Pandis, S.N., Barnes, I., 2005. Organic aerosol and global climate modelling: a review. *Atmospheric Chem. Phys.* 5, 1053–1123. doi:10.5194/acp-5-1053-2005

- Kleinman, L.I., Springston, S.R., Wang, J., Daum, P.H., 2009. The time evolution of aerosol size distribution over the Mexico City plateau. *Atmospheric Chem. Phys.* 9, 4261–4278.
- Knipping, E.M., Lakin, M.J., Foster, K.L., Jungwirth, P., 2000. Experiments and Simulations of Ion-Enhanced Interfacial Chemistry on Aqueous NaCl Aerosols. *Science* 287, 301.
- Lalithambika, K.C., Thayumanvan, A., Sriram, S., 2016. Density functional analysis of adsorption of NO₂ on ZnSe nano structures. *Pharma Chem.* 8, 441–448.
- Levin, Z., Cotton, W.R., 2009. *Aerosol pollution impact on precipitation: a scientific review*, 1. Aufl. ed. Springer, Dordrecht.
- Mason, B.J., 1954. Bursting of Air Bubbles at the Surface of Sea Water. *Nature* 174, 470–471. doi:10.1038/174470a0
- Massel, S.R., 2007a. *Fundamentals of marine aerosols*, in: *Ocean Waves Breaking and Marine Aerosol Fluxes*, Atmospheric and Oceanographic Science Library. Springer New York, pp. 207–228.
- Massel, S.R., 2007b. *Basic processes near the air–sea interface*, in: *Ocean Waves Breaking and Marine Aerosol Fluxes*, Atmospheric and Oceanographic Science Library. Springer New York, pp. 1–9.
- Orellana, M.V., Verdugo, P., 2003. Ultraviolet Radiation Blocks the Organic Carbon Exchange between the Dissolved Phase and the Gel Phase in the Ocean. *Limnol. Oceanogr.* 48, 1618–1623.
- Ottosson, N., 2011. *Aqueous Solutions as seen through an Electron Spectrometer. Surface Structure, Hydration Motifs and Ultrafast Charge Delocalization Dynamics* (Doctoral thesis). Uppsala university, Uppsala.
- Petersen, P.B., Saykally, R.J., 2006. On the nature of ions at the liquid water surface. *Annu. Rev. Phys. Chem.* 57, 333–364. doi:10.1146/annurev.physchem.57.032905.104609
- Powell, C.J., Jablonski, A., 2009. Surface sensitivity of X-ray photoelectron spectroscopy. *Nucl. Inst Methods Phys. Res. A* 601, 54–65. doi:10.1016/j.nima.2008.12.103
- Powell, C.J., Jablonski, A., 1999. Evaluation of Calculated and Measured Electron Inelastic Mean Free Paths Near Solid Surfaces. *J. Phys. Chem. Ref. Data* 28, 19–62. doi:10.1063/1.556035
- Prisle, N.L., Ottosson, N., Öhrwall, G., Söderström, J., Dal Maso, M., Björneholm, O., 2012. Surface/bulk partitioning and acid/base speciation of aqueous decanoate: direct observations and atmospheric implications. *Atmos Chem Phys* 12, 12227–12242. doi:10.5194/acp-12-12227-2012
- Prisle, N.L., Raatikainen, T., Laaksonen, A., Bilde, M., 2010. Surfactants in cloud droplet activation: mixed organic-inorganic particles. *Atmospheric Chem. Phys.* 10, 5663.
- Richmond, G.L., 2002. Molecular Bonding and Interactions at Aqueous Surfaces as Probed by Vibrational Sum Frequency Spectroscopy. *Chem. Rev.* 102, 2693–2724. doi:10.1021/cr0006876
- Riley, G.A., 1963. Organic Aggregates in Seawater and the Dynamics of Their Formation and Utilization. *Limnol. Oceanogr.* 8, 372–381.
- Rogge, W.F., Hildemann, L.M., Mazurek, M.A., Cass, G.R., Simoneit, B.R.T., 1993. Sources of fine organic aerosol. 2. Nuncatalyst and catalyst-equipped automobiles and heavy-duty diesel trucks. *Environ. Sci. Technol.* 27, 636–651. doi:10.1021/es00041a007
- Rohli, R.V., Vega, A.J., 2015. *Climatology*, 3rd ed. Jones & Bartlett Learning.
- Seidel, R., Thürmer, S., Winter, B., 2011. Photoelectron Spectroscopy Meets Aqueous Solution: Studies from a Vacuum Liquid Microjet. *J. Phys. Chem. Lett.* 2, 633–641. doi:10.1021/jz101636y
- Siegbahn, K., 1981. *Electron spectroscopy for atoms, molecules and condensed matter*, Nobel lecture.

- Siegbahn, K., Nordling, C., Fahlman, A., Nordberg, R., Hamrin, K., Hedman, J., Johansson, G., Bergmark, T., Karlsson, S.-E., Lindgren, I., Lindberg, B., 1967. *Atomic, Molecular and Solid State Structure Studied by Means of Electron Spectroscopy*. Nova Acta Regiae Soc. Sci. Upsaliensis.
- Vaida, V., 2011. Perspective: Water cluster mediated atmospheric chemistry. *J. Chem. Phys.* 135, 20901. doi:10.1063/1.3608919
- Van der Heide, P., 2012. *X-ray photoelectron spectroscopy: an introduction to principles and practices*. Wiley, Hoboken, N.J.
- Wagner, J.M., 2010. *X-Ray Photoelectron Spectroscopy, Chemical Engineering Methods and Technology*. Nova.
- Walz, M.-M., Caleman, C., Werner, J., Ekholm, V., Lundberg, D., Prisle, N.L., Öhrwall, G., Björneholm, O., 2015. Surface behavior of amphiphiles in aqueous solution: a comparison between different pentanol isomers. *Phys Chem Chem Phys* 17, 14036–14044. doi:10.1039/C5CP01870F
- Walz, M.-M., Werner, J., Ekholm, V., Prisle, N.L., Öhrwall, G., Björneholm, O., 2016. Alcohols at the aqueous surface: chain length and isomer effects. *Phys. Chem. Chem. Phys. PCCP* 18, 6648–6656. doi:10.1039/c5cp06463e
- Wenger, D., 2015. *Acid and Base Behaviour in Water Clusters* (Bachelor thesis). Uppsala university, Uppsala.
- Werner, J., 2015. *Exploring the Surface of Aqueous Solutions: X-ray photoelectron spectroscopy studies using a liquid micro-jet* (Doctoral thesis). Uppsala university, Uppsala.
- Willmott, P., 2011. *An Introduction to Synchrotron Radiation : Techniques and Applications*. Wiley.
- Winter, B., 2009. Liquid microjet for photoelectron spectroscopy. *Nucl. Instrum. Methods Phys. Res. Sect. Accel. Spectrometers Detect. Assoc. Equip., Special issue in honour of Prof. Kai Siegbahn* 601, 139–150. doi:10.1016/j.nima.2008.12.108
- Yancey, P.H., Clark, M.E., Hand, S.C., Bowlus, R.D., Somero, G.N., 1982. Living with Water Stress: Evolution of Osmolyte Systems. *Science* 217, 1214–1222.

8. INTERNET REFERENCES

- Gromacs, Abraham, M.J., 2017. *Gromacs - Gromacs*. URL <http://www.gromacs.org/> [5.24.17].
- Gromacs, Abraham, M.J., 2010. *OPLS - Gromacs*. URL http://www.gromacs.org/Documentation/Terminology/Force_Fields/OPLS [5.24.17].
- Helms, I., 2015. *Electron Storage Ring BESSY II. Electron Storage Ring BESSY II- Descr. Funct.* URL https://www.helmholtz-berlin.de/quellen/bessy/elektronenspeicherring/index_en.html [9.16.16].
- Schrödinger, 2016. *PyMOL / www.pymol.org*. URL <https://www.pymol.org/> [10.19.16].
- Scienta, 2016. *Products - Scienta Omicron GmbH*. URL <http://www.scientaomicron.com/en/products/354/1229> [10.19.16].
- sklogwiki, 2015. *SPC/E model of water page on SklogWiki - a wiki for statistical mechanics and thermodynamics*. URL http://www.sklogwiki.org/SklogWiki/index.php/SPC/E_model_of_water [1.31.17].
- WaveMetrics, 2016. *WaveMetrics - scientific graphing, data analysis, curve fitting & image processing software*. URL <https://www.wavemetrics.com/index.html> [10.19.16].

APPENDIX A. STABILITY MEASUREMENTS

The stability measurements of the 1:75 (glycerol: water) ratio are depicted in (Figure 13). The measurements are similar to each other but there is a small difference between that is lower, around or above 5%. For example the three points with the largest difference are given in Table 4. Two of the points had a larger difference than 5%; 7.8% and 6.5%, however the stability is determined with the whole curve and a few points above 5% does not matter.

Table 4. The three points with the largest difference between them for the 1 glycerol: 75 water experiment

Y coordinate after the measurements	Y coordinate before the measurements	X coordinate	Percentage of the difference between measurements
19787	20692	8.3	4.4
8752.3	9494.4	14.5	7.8
17280	18551	27.7	6.5

The difference is larger at the peaks but decreases directly afterwards. It is always the spectra before the measurements that has the highest values.

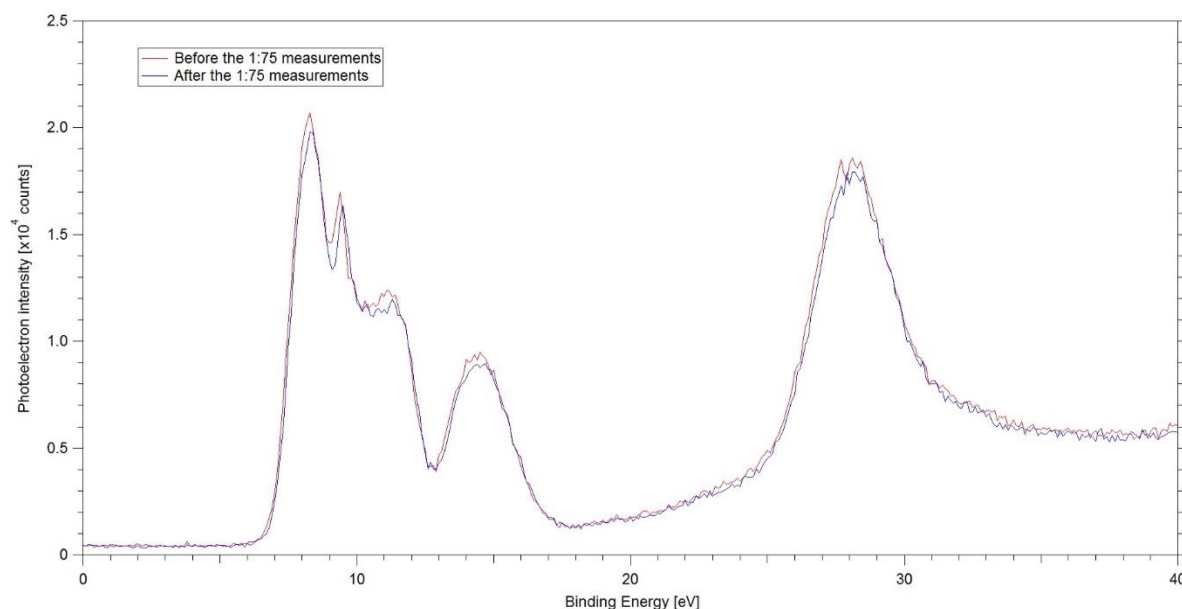


Figure 13. The water spectra for the stability measurements of the ratio 1 glycerol: 75 water. The PE signal is on the y-axis and the Electron BE is at the x-axis (eV)

The stability measurements of the 1:35 (glycerol: water) ratio are depicted in Figure 14. The measurements are similar to each other but there is a small difference between them that is lower than or around 5%, although there are differences a bit larger than 5%. For example the three points with the largest difference are given in Table 5 one of the points had a larger difference than 5%, that point had a difference of 9.1%, however the stability is determined with the whole curve and one point above 5% does not matter.

Table 5. The three points with the largest difference between them for the 1 glycerol: 35 water experiment

Y coordinate after the measurements	Y coordinate before the measurements	X coordinate	Percentage of the difference between measurements
20069	20747	8.4	3.3
11002	12109	11.6	9.1

The difference is about the same the whole spectra except at a few peaks. The spectrum before and after takes turns of having the largest values.

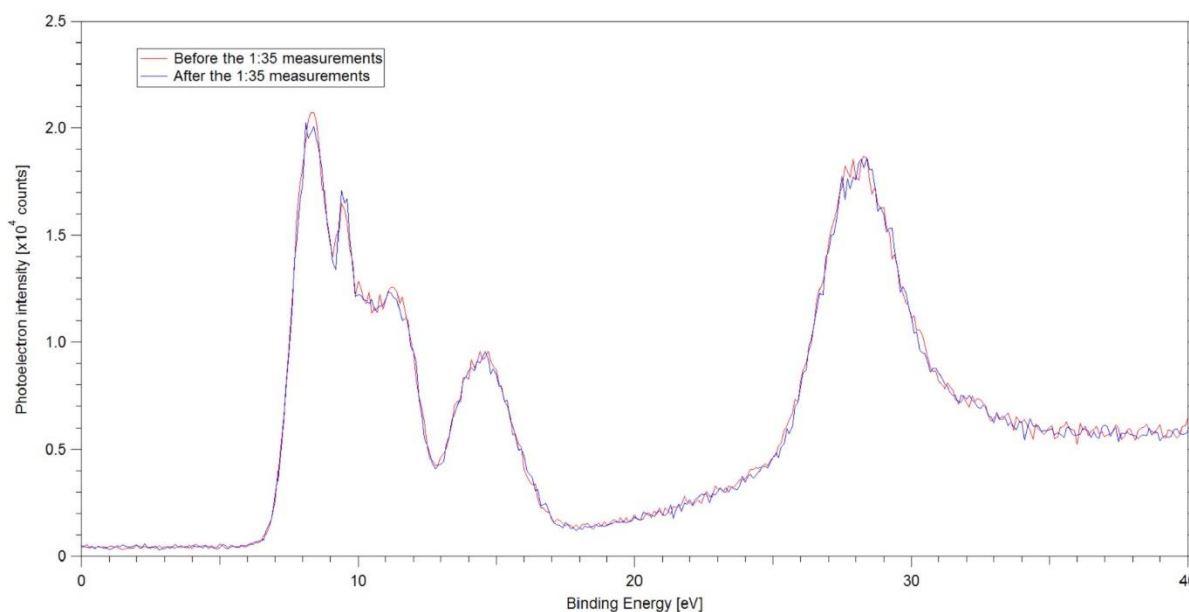


Figure 14. The water spectra for the stability measurements of the ratio 1 glycerol: 35 water. The PE signal is on the y-axis and the Electron BE is at the x-axis (eV)

The stability measurements of the 1:8 (glycerol: water) ratio are depicted in Figure 15. The measurements are similar to each other but there is a small difference between them that is lower or around 5%, a few measurement points have a larger difference than 5%. For example the three points with the largest difference are given in Table 6. One of the points had a larger difference than 5%, that point had a difference of 8.6%, however the stability is determined with the whole curve and one point above 5% does not matter.

Table 6. The three points with the largest difference between them for the 1 glycerol: 8 water experiment

Y coordinate after the measurement	Y coordinate before the measurement	X coordinate	Percentage of the difference between measurements
17886	17007	9.4	4.9
13525	12365	10.1	8.6
20079	19318	28.2	3.8

The largest differences are at the peaks and to the left of 30 eV of the BE (Figure 15). The spectra after the measurement mostly had the highest values.

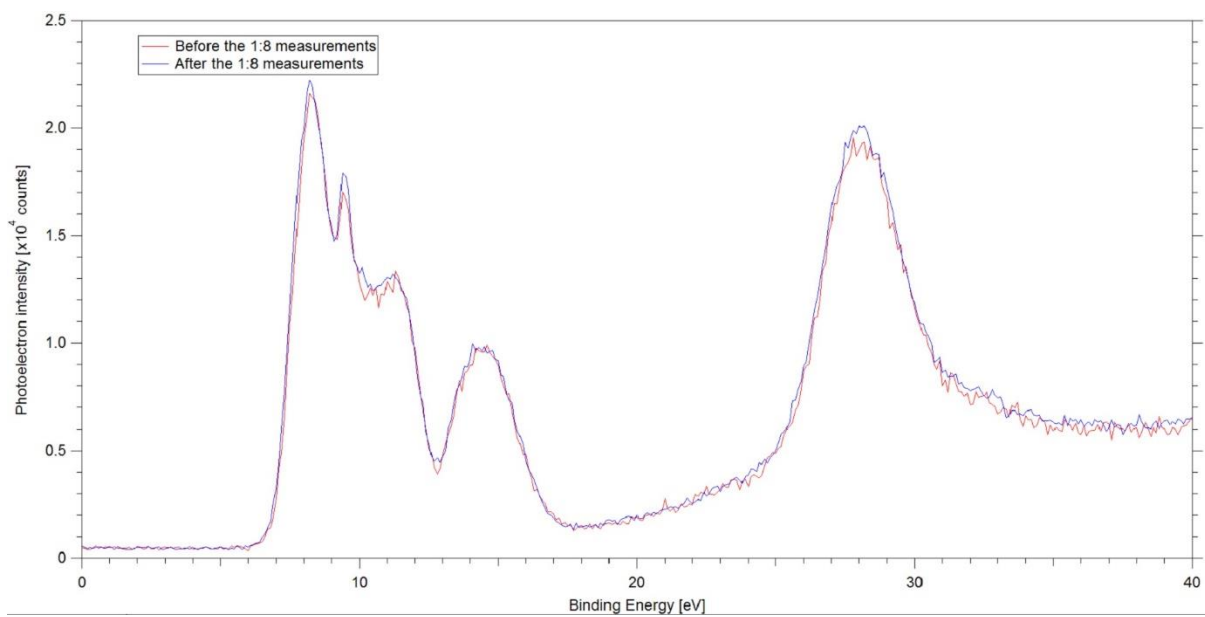


Figure 15. The water spectra for the stability measurements of the ratio 1 glycerol: 8 water. The PE signal is on the y-axis and the Electron BE is at the x-axis (eV)